Philosophical Magazine A

ISSN: 0141-8610 (Print) 1460-6992 (Online) Journal homepage: http://www.tandfonline.com/loi/tpha20

A dislocation-based analysis of strain history effects in ice

David. M. Cole & Glenn. D. Durell

To cite this article: David. M. Cole & Glenn. D. Durell (2001) A dislocation-based analysis of strain history effects in ice, Philosophical Magazine A, 81:7, 1849-1872, DOI: 10.1080/01418610108216640

To link to this article: http://dx.doi.org/10.1080/01418610108216640

PHILOSOPHICAL MAGAZINE A, 2001, VOL. 81, NO. 7, 1849–1872

A dislocation-based analysis of strain history effects in ice

DAVID M. COLE† and GLENN D. DURELL

US Army Cold Regions Research and Engineering Laboratory, Hanover, New Hampshire, USA

[*Received 6 December 1999 and accepted in revised form 20 October 2000*]

ABSTRACT

The cyclic loading response of ice specimens can be analysed with a dislocation-based model of anelasticity to produce an estimate of the effective mobile dislocation density. Moreover, the cyclic loading response is sufficiently sensitive to track the dislocation density changes that occur during creep straining. A combination of cyclic and creep loading experiments can thus be employed to gain crucial insight regarding the relationship between the dislocation density that evolves during creep straining and the anelastic and viscous components of strain. Creep and cyclic loading experiments have been conducted on laboratory-prepared saline and freshwater ice specimens to shed light on the effects of temperature, creep stress and accumulated strain on the mobile dislocation density and thereby to support the further development of a physically based constitutive model for ice. The findings indicate that, in addition to the expected stress and strain dependence, the dislocation density that develops during straining also depends on the temperature and microstructure. As a consequence of this temperature dependence, the apparent activation energy for creep when dislocation multiplication takes place is higher than that for creep in the absence of dislocation multiplication. Data from the literature are examined and found to support this finding. The results indicate that both the anelastic strain and the viscous strain rate vary with the mobile dislocation density. A preliminary set of results indicates that the power law stress exponent n is 3 when the applied stress is high enough to cause an increase in the dislocation density, but that $n \approx 1$ when the dislocation density remains constant during straining. The results show that prior straining increases the stress level associated with the transition from $n = 1$ to $n = 3$. The findings provide support for the glide-controlled mechanism of ice creep, and a dislocation glide-based formulation for viscous straining is presented. The model agrees well with the experimental data in the pure flow regime.

§1. INTRODUCTION

It has been recognized for some time that the dislocation density in ice, as in many crystalline solids, increases during straining and that dislocations play a significant role in ice deformation. However, dislocation-based mechanisms have not been fully absorbed into constitutive models of ice because dislocation processes are difficult to quantify and, perhaps more fundamentally, the rate-controlling deformation mechanism has not been clearly identified. The work discussed below addresses those two issues. Experimental and analytical results are presented that quantify the

† E-mail: David.M.Cole@erdc.usace.army.mil

Philosophical Magazine A ISSN 0141–8610 print/ISSN 1460-6992 online © 2001 Taylor & Francis Ltd
http://www.tandf.co.uk/journals
DOI: 10.1080/01418610010019116

effective mobile dislocation density in ice specimens and illustrate that the key features of ice deformation (anelastic and viscous strain) are closely tied to the dislocation density. The observations support a dislocation glide-controlled mechanism of deformation and thus provide valuable insight for the further development of a dislocation-based constitutive model for sea ice. Example results for freshwater ice show that the fundamental processes under discussion are applicable to that material as well.

The dislocation-based model of anelasticity presented by Cole (1995) provides a means to calculate an effective dislocation density from the hysteresis loops observed during reversed direct-stress (cyclic tension–compression) experiments. By applying both cyclic and creep loading methods to a single specimen, it is possible to use the cyclic loading response to quantify changes in its dislocation density as a function of creep strain. This indirect approach is necessary in part because of the difficulty in making direct observations of dislocations in ice specimens having a statistically significant number of grains. The stress levels and frequency of the load cycles were selected so that the specimens were not perceptibly altered as a result of the cyclic loads, and to assure that the cyclic loading response was dominated by the recoverable motion of dislocations.

The paper presents experimental results for test temperatures of −20, −15, −10 and −5°C, and uniaxial compressive creep stresses in the range 0.3–2.9 MPa. Significantly, the analysis reveals that the viscous strain rate typically varied during primary creep, and the variations generally parallelled those of the calculated dislocation density. This provides justification for quantifying the viscous as well as the anelastic component of strain in terms of an effective dislocation density.

One of the objectives of the constitutive modelling effort is to relate the mechanical behaviour directly to the physical properties of sea ice. The experimental results presented below provide further substantiation of a relationship that was found in previous work to exist between the initial dislocation density of a specimen and its salinity. A subsequent publication will incorporate the findings presented here into the dislocation-based model of Cole (1995, 1998), and a preliminary treatment has appeared in the paper by Cole and Durell (1998).

§2. Background

Dislocation multiplication has long been observed in freshwater ice (Fukuda and Higashi 1969, Shearwood and Whitworth 1991, Hu *et al.* 1996), and the importance of dislocations in the mechanical behaviour of ice has been recognized for many years (Homer and Glen 1978, Vassoille *et al.* 1978). Ice studies employing X-radiation topography have generally focused on laboratory-prepared single crystals or polycrystals with very few grains, having a very low initial dislocation density, and subjected to relatively low total strains. Although similar studies in sea ice have apparently not been conducted, preliminary attempts (I. Baker 1999, private communication) indicate that the number of dislocations in unstrained sea ice is so high that direct observations are difficult. Bright field imaging, for example, is effective for dislocation densities up to approximately $1 \times 10^9\,\mathrm{m}^{-2}$, which is of the order of the values calculated below for typical unstrained sea ice specimens. It is anticipated that weak-beam imaging, useful for dislocation densities of up to $2 \times 10^{10}\,\mathrm{m}^{-2}$, depending on the dislocation geometries (Barrett *et al.* 1995), may be applicable to strained sea ice.

The indication that dislocations exist in great numbers in sea ice is fully consistent with the experimentally observed high compliance of sea ice relative to freshwater ice (Cole 1998). The reason why the dislocation density of undeformed sea ice is significantly higher than freshwater ice is most probably rooted in differences in the growth habits of the two materials and/or the effects of temperature changes on the liquid brine inclusions in the sea ice microstructure. Sea ice grows dendritically, with a very convoluted ice–water interface, and it seems possible that the relatively thin (e.g. less than 1 mm) plates in the skeletal layer would be subjected to sufficient deformation during the growth process to generate dislocations. Additionally, temperature fluctuations cause phase changes (and an associated volume change) in the brine inclusions in sea ice. The calculations of Picu *et al.* (1994) indicated that the stresses generated by this process can be as high as several megapascals, which is sufficient to produce dislocations.

The experiments presented below employ a patented gripping system (Cole and Gould 1990) for applying fully reversed uniaxial load cycles to cylindrical ice specimens. When used in conjunction with a closed-loop electrohydraulic testing machine, these grips make it possible to switch freely from quasistatic tension or compression loading to cyclic loading paths and thus make possible the types of experiment described below. Cole (1993) presented the results of laboratory experiments that examined two approaches to combining cyclic loading with standard creep loading methods. One approach subjected a specimen to several periods of creep loading, allowing time for recovery after each loading period. Sets of sinusoidal zero-mean-stress cycles were applied between each creep loading period as well as before and after the entire loading sequence. An analysis of the area of these loops provided a means to quantify the increase in anelasticity (loss compliance) with accumulated creep strain, and the anelasticity in turn can be related to the dislocation density. In the second approach, the load cycles were superimposed on the creep stress. The two approaches produced essentially the same information; the creep deformation produced an increase in the anelastic compliance of specimens, the compliance increase was due to an increase in the mobile dislocation density during primary creep, and the cyclic loading response was sufficiently sensitive to quantify the observed behaviour. The anelastic compliance, and hence the dislocation density, typically reached a nominally constant value during the first 0.01 of creep strain, with most of the increase occurring before $\varepsilon = 0.005$. This strain dependence is reflected in both the hysteresis loop areas and the level of anelastic strain observed during creep recovery.

The staged creep loading method provides a way to track changes in the total anelastic strain and the viscous strain rate as a function of accumulated viscous strain. The average viscous strain rate for each loading stage can be calculated directly from the permanent strain at the end of each loading segment (without influence from simultaneously occurring anelastic strain). Characteristics of the hysteresis loops (the loop area, the loop width along the x-axis, and the slope) and the internal friction ϕ (the ratio of the hysteresis loop area to the peak strain energy during a load cycle) obtained under cyclic loading provide a means to quantify changes induced by the creep deformation. Internal friction is a dimensionless measure of the energy dissipated per loading cycle, and it is dominated by anelastic strain under the prevailing conditions. This quantity is especially useful for comparing anelasticity observed under cyclic and quasistatic loading conditions.

§3. Experimental details

The laboratory experiments employed the reversed direct-stress testing method presented by Cole and Durell (1995), and the procedures described by Cole (1993). The experimental technique provides a means to apply uniaxial tension–compression loading to cylindrical ice specimens. The cyclic loading conditions (peak stresses and frequency) were selected to result in a constant-microstructure test (e.g. a test in which no measurable change occurs in the microstructure during load cycling). A set of load cycles were applied prior to creep deformation to assess the initial state of each specimen. A loading sequence was then applied that consisted of creep loading for a total strain of about 0.0025, load removal, anelastic strain recovery, and sets of loading cycles. This sequence was repeated several times under a single creep stress level σ_{creep} until the accumulated creep strain ε_{creep} was approximately 10^{-2}. The cyclic loading frequency was 0.1 Hz, which was sufficiently low to produce measurable anelastic strain, but high enough to avoid the complicating effects of cyclic viscous strain. The peak cyclic stresses were typically $\sigma_{cyc} = \pm 0.1$, ± 0.2 and ± 0.3 MPa, with specimens tested at higher temperatures being subjected to lower peak stresses. Since zero-mean-stress cycles were being employed, the peak cyclic stress was limited by a conservative estimate of the tensile strength of the ice, which can be as low as 0.4 MPa for the material being tested.

Most of the specimens (those beginning with the letters NP) were produced in the laboratory and prepared for testing using the methods given by Cole and Durell (1995). Briefly, they were grown from water having a bulk salinity of 15–17 ppt and containing the six most prevalent salts in seawater in the proportions that occur in nature. The freezing rate was approximately 25 mm day^{-1}. This combination of salinity and freezing rate in the laboratory produces specimens with a microstructure and bulk salinity that are close to those of naturally occurring sea ice. Freezing was accomplished from the top down using a cold plate, and its temperature was periodically decreased during the freezing process to maintain an approximately constant freezing rate. Table 1 gives the physical properties and test temperatures for the specimens. Core specimens measuring 100 mm in diameter, approximately 250 mm in length and oriented with their long axis perpendicular to the growth direction, were obtained from the blocks and generally tested within a matter of days after growth of the parent ice block. The cyclic loading method involves relatively low strains and therefore requires a very precise monitoring system. The deformation monitoring system thus employed high-resolution specimen-mounted displacement transducers to provide a strong signal and to avoid the effects of end conditions on the measurements.

Data are included from experiments on a field core of first-year sea ice and laboratory-prepared granular freshwater ice. Those experiments elucidate the dislocation density–stress relationship and support the theoretical implications of the model with regard to the influence of dislocation density on the transition to linear behaviour. Cole *et al.* (1998) gave the background of the sea ice specimen.

§4. Results

Table 2 lists the accumulated viscous strain, the calculated dislocation density ρ, the average viscous strain rate $\dot{\varepsilon}_{visc}$ and the anelastic strain $\varepsilon_{anelastic}$ observed for each segment. The calculated dislocation density and internal friction ϕ (determined from the cyclic loading results) were calculated for the initial state ($\varepsilon_{visc} = 0$) and at the end of each creep loading segment. The experiments examined primary creep;

Table 1. Physical properties of the specimens.

Specimen	Test temperature (°C)	Salinity (ppt)	Bulk density ($Mg\,m^{-3}$)	Porosity		
				Brine at test temperature	Gas	Total
NP14	−5	5.5	0.9	0.022	0.027	0.049
NP22	−5	4.1	0.890	0.039	0.016	0.075
NP23	−5	3.7	0.879	0.035	0.014	0.082
NP32	−5	5.0	0.889	0.020	0.038	0.058
NP43	−5	4.9	0.894	0.020	0.032	0.052
NP72	−10	7.0	0.902	0.028	0.026	0.054
NP73	−10	6.8	0.883	0.027	0.046	0.073
NP82	−10	7.2	0.914	0.029	0.013	0.043
NP94	−10	7.5	0.914	0.041	0.0306	0.053
NP11	−15	8.1	0.908	0.033	0.033	0.054
NP21	−15	4.6	0.888	0.018	0.018	0.053
NP62	−15	7.5	0.902	0.030	0.027	0.057
NP64	−15	8.0	0.883	0.031	0.048	0.079
NP92	−15	6.1	0.898	0.024	0.029	0.054
NP36	−20	5.5	0.897	0.018	0.022	0.043
NP44	−20	6	0.892	0.02	0.026	0.05
NP45	−20	6.6	0.886	0.021	0.024	0.058
NP46	−20	6.2	0.894	0.02	0.025	0.048

specimens were typically tested to a total axial strain of about 0.01, and the maximum viscous strain was about 0.008.

Figure 1 illustrates a typical set of curves for the four creep loading segments applied to a specimen tested at −20°C, and the associated cyclic loading results. The increasing hysteresis loop area in figure 1 (*b*) evidences the effect of the creep straining on the cyclic loading response. Each set of hysteresis loops consists of three cycles of zero-mean-stress sinusoidal loading, and they have been shifted arbitrarily along the strain axis for clarity. The curve labelled Pre-creep was obtained prior to the first creep loading segment and thus represents the as-grown condition. The other curves were obtained after each of the subsequent creep loading segments.

Figure 2 plots internal friction as a function of viscous strain for specimens tested at temperatures of −10 and −20°C, with creep stress levels indicated in the keys. The initial internal friction values vary owing to differences in the physical properties of the specimens. These results show that the most significant increase in internal friction typically occurred over the first segment of creep straining (up to $\varepsilon_{tot} \approx 0.001$), followed by a more gradual increase with subsequent straining.

Figure 3 plots representative data from table 2 as a function of the accumulated viscous strain. Significantly, and with few exceptions, there was a trend at all temperatures for ρ, $\dot{\varepsilon}_{visc}$, ϕ and $\varepsilon_{anelastic}$ either to increase or to decrease together as viscous straining proceeded. For most of the experiments conducted at −10, −15 and −20°C, the values of ρ, $\dot{\varepsilon}_{visc}$, ϕ and $\varepsilon_{anelastic}$ increase with increasing creep strain, tending to an apparent plateau value by the end of primary creep. The initial (pre-creep) values of internal friction and dislocation density (ϕ_0 and ρ_0) increased with

Table 2. Summary of experimental results.

Strain	Temperature (°C)	Creep stress (MPa)	Viscous strain	Dislocation density (10^9 m^{-2})	Internal friction	Viscous strain rate (s^{-1})	Anelastic strain
NP32	−5	−1.50	0	4	0.183		
			0.001 2	5.8	0.192	1.530×10^{-4}	1.303×10^{-3}
			0.003 2	5.2	0.210	1.560×10^{-4}	1.588×10^{-3}
			0.005 9	4.7	0.208	1.189×10^{-4}	1.655×10^{-3}
			0.007 5	3.4	0.206	1.175×10^{-4}	1.428×10^{-3}
NP14	−5	−0.52	0	4.6	0.201		
			0.001 5	4.6	0.183	8.575×10^{-6}	9.011×10^{-4}
			0.004 0	4	0.217	3.955×10^{-6}	1.003×10^{-3}
			0.006 5	4	0.210	1.993×10^{-6}	9.782×10^{-4}
			0.008 0	3.8	0.231	1.833×10^{-6}	9.536×10^{-4}
NP22	−5	−0.98	0	4.3	0.165		
			0.001 2	6.2	0.213	7.463×10^{-5}	1.210×10^{-3}
			0.003 4	5.9	0.233	6.039×10^{-5}	1.580×10^{-3}
			0.005 7	5.6	0.213	4.764×10^{-5}	1.740×10^{-3}
			0.007 3	7.8	0.243	4.207×10^{-5}	1.640×10^{-3}
NP23	−5	−0.29	0	2.5	0.170		
			0.003 1	2.2	0.182	1.961×10^{-7}	4.654×10^{-4}
			0.005 5	2.4	0.197	1.769×10^{-7}	5.233×10^{-4}
			0.008 3	2.5	0.181	1.774×10^{-7}	5.196×10^{-4}
			0.009 7	2.7	0.209	1.481×10^{-7}	5.410×10^{-4}
NP43	−5	−0.29	0	4.5	0.189		
			0.001 6	7	0.235	1.169×10^{-5}	2.463×10^{-3}
			0.004 0	5.5	0.229	5.542×10^{-6}	3.317×10^{-3}
			0.006 5	5.5	0.229	3.021×10^{-6}	1.043×10^{-3}
			0.008 0	5.7	0.238	2.048×10^{-6}	1.014×10^{-3}
NP73	−10	−0.48	0	4	0.157		
			0.001 7	4.8	0.198	1.167×10^{-6}	7.485×10^{-4}
			0.004 2	5	0.204	4.430×10^{-7}	7.881×10^{-4}
			0.006 9	5.7	0.199	3.381×10^{-7}	7.326×10^{-4}
			0.008 6	5.6	0.203	6.974×10^{-7}	8.319×10^{-4}
NP94	−10	−0.91	0	4.7	0.187		
			0.001 4	6.8	0.249	3.557×10^{-5}	1.000×10^{-3}
			0.003 6	7.8	0.245	3.313×10^{-5}	1.500×10^{-3}
			0.006 0	8	0.256	3.692×10^{-5}	1.460×10^{-3}
			0.007 8	8.5	0.233	4.410×10^{-5}	1.230×10^{-3}
NP82	−10	−1.41	0	5.6	0.219		
			0.001 2	7.8	0.221	9.992×10^{-5}	1.301×10^{-3}
			0.003 3	8.9	0.237	1.040×10^{-4}	1.659×10^{-3}
			0.005 7	8.3	0.220	1.113×10^{-4}	1.921×10^{-3}
			0.007 4	8.9	0.222	9.409×10^{-5}	1.761×10^{-3}
NP72	−10	−1.81	0	4.3	0.162		
			0.001 0	6.4	0.196	7.777×10^{-5}	1.343×10^{-3}
			0.003 2	6.6	0.218	1.091×10^{-4}	1.754×10^{-3}
			0.005 6	7.2	0.219	1.102×10^{-4}	1.863×10^{-3}
			0.007 2	8	0.226	1.030×10^{-4}	1.784×10^{-3}
NP64	−15	−1.41	0	3.2	0.152		
			0.001 3	4.5	0.200	2.926×10^{-5}	1.070×10^{-3}

(*Continued*)

Table 2. (*Continued*).

Strain	Temperature (°C)	Creep stress (MPa)	Viscous strain	Dislocation density (10^9 m^{-2})	Internal friction	Viscous strain rate (s^{-1})	Anelastic strain
NP64			0.003 5	4.5	0.178	1.612×10^{-5}	1.370×10^{-3}
			0.005 9	4.5	0.160	1.979×10^{-5}	1.560×10^{-3}
			0.007 4	4.5	0.196	2.232×10^{-5}	1.520×10^{-3}
NP92	−15	−0.96	0	3.2	0.053		
			0.001 3	4.7	0.113	7.379×10^{-6}	1.116×10^{-3}
			0.003 5	5.2	0.115	4.735×10^{-6}	1.448×10^{-3}
			0.005 9	5.2	0.133	4.422×10^{-6}	1.591×10^{-3}
			0.007 6	5	0.130	8.252×10^{-6}	1.337×10^{-3}
NP62	−15	−2.01	0	3.4	0.138		
			0.001 1	4.7	0.186	6.865×10^{-5}	1.257×10^{-3}
			0.003 2	4.7	0.192	8.142×10^{-5}	1.590×10^{-3}
			0.005 9	4.7	0.195	9.327×10^{-5}	1.667×10^{-3}
NP11	−15	−1.52	0	3.2	0.139		
			0.001 1	4.7	0.172	3.200×10^{-5}	1.228×10^{-3}
			0.003 3	5.7	0.197	3.819×10^{-5}	1.643×10^{-3}
			0.005 7	5.5	0.210	4.177×10^{-5}	1.743×10^{-3}
			0.007 4	6.8	0.198	4.207×10^{-5}	1.802×10^{-3}
NP21	−15	−2.49	0	2.5	0.136		
			0.000 9	3.6	0.183	5.927×10^{-5}	1.204×10^{-3}
			0.003 1	5	0.206	8.546×10^{-5}	1.734×10^{-3}
			0.005 6	5.9	0.206	1.029×10^{-4}	1.875×10^{-3}
			0.007 2	6.8	0.227	9.406×10^{-5}	1.791×10^{-3}
NP36	−20	−2.49	0	4	0.140		
			0.000 8	7	0.172	8.299×10^{-5}	2.039×10^{-3}
			0.002 9	7	0.180	7.577×10^{-5}	1.895×10^{-3}
NP44	−20	−1.97	0	2.3	0.128		
			0.001 1	3	0.160	2.681×10^{-5}	1.237×10^{-3}
			0.003 1	3.5	0.168	3.163×10^{-5}	1.690×10^{-3}
			0.005 5	4.1	0.174	3.792×10^{-5}	1.829×10^{-3}
			0.007 4	4.1	0.175	4.474×10^{-5}	1.497×10^{-3}
NP45	−20	−2.95	0	3.5	0.141		
			0.001 0	6	0.201	1.073×10^{-4}	1.319×10^{-3}
			0.003 0	7.1	0.194	1.573×10^{-4}	1.870×10^{-3}
			0.005 3	10	0.198	1.636×10^{-4}	2.086×10^{-3}
			0.006 9	8.5	0.203	1.020×10^{-4}	1.971×10^{-3}
NP46	−20	−2.46	0	3.1	0.135		
			0.000 9	4.9	0.177	6.141×10^{-5}	1.400×10^{-3}
			0.002 7	6.3	0.201	8.972×10^{-5}	2.107×10^{-3}
			0.004 9	7.3	0.218	9.089×10^{-5}	2.382×10^{-3}
			0.006 6	6.5	0.215	1.013×10^{-4}	2.331×10^{-3}
GKD6	−10	−0.8	0	0.71	0.142		
			0.002 359	0.75	0.147	2.09×10^{-6}	8.56×10^{-4}
(columnar freshwater ice;			0.004 729	1.35	0.148	2.39×10^{-6}	1.54×10^{-3}
loading axis is 45° to columns;			0.008 666	1.58	0.186	2.54×10^{-6}	1.53×10^{-3}
first loading $\sigma_{creep} = 1$ MPa)			0.012 857	2	0.235	4.56×10^{-6}	1.16×10^{-3}
APX-1	−10	−2.4	0	0.55	0.076		
			0.000 018 4	0.62	0.084	2.831×10^{-6}	2.35×10^{-4}
(granular freshwater ice;			0.000 178 7	0.79	0.098	2.949×10^{-6}	5.70×10^{-4}
grain size, approximately 5 mm)			0.003 394 3	1.78	0.168	3.338×10^{-6}	1.23×10^{-3}

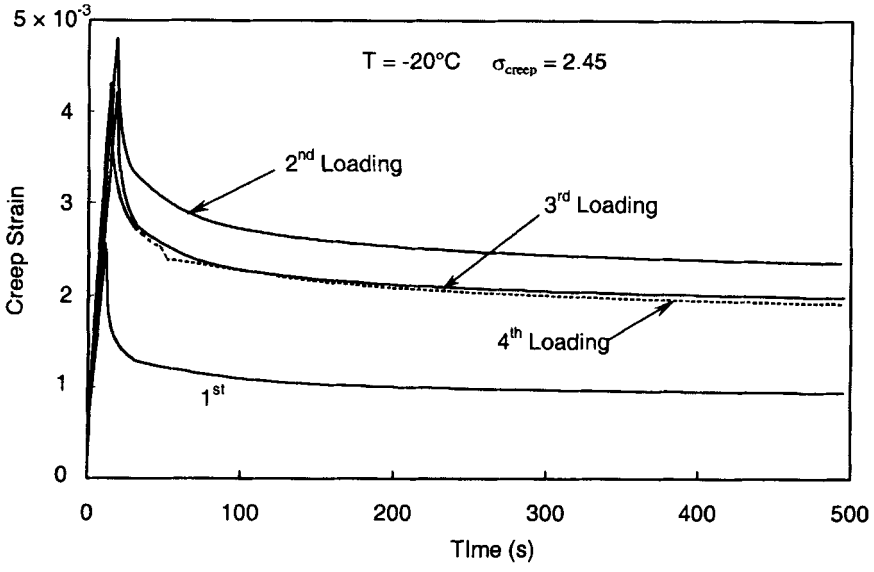

(*a*)

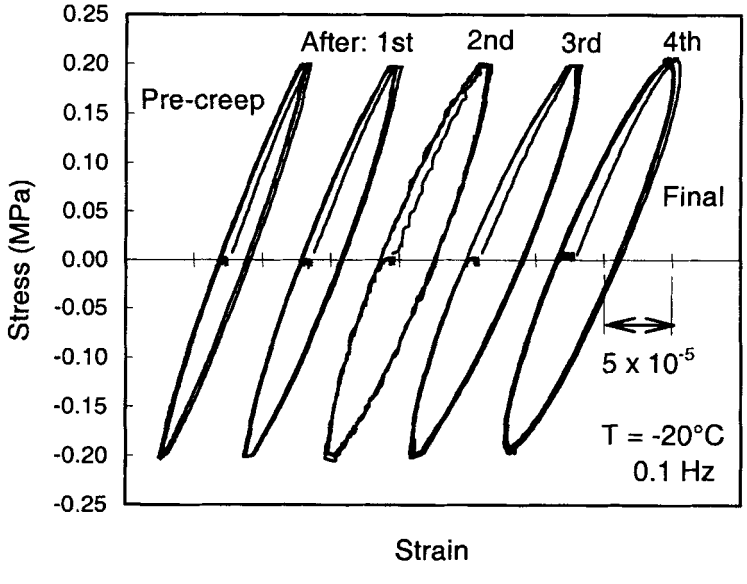

(*b*)

Figure 1. (*a*) Typical creep curves for the conditions indicated. The time under load for each creep loading segment was 14.5, 20.4, 23.6 and 16.8 s. The total creep strain increment in each segment was −0.002 55, −0.004 19, −0.004 79 and −0.00 43. (*b*) Typical hysteresis loops obtained prior to creep loading (pre-creep) and after each subsequent creep loading segment shown in (*a*).

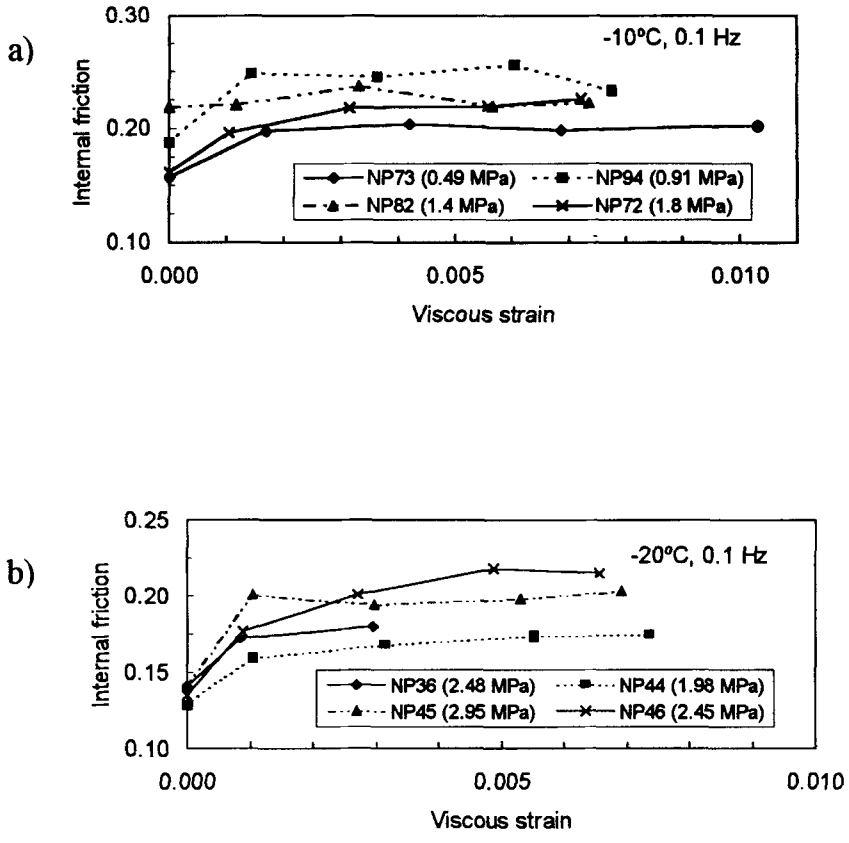

Figure 2. Internal friction versus accumulated viscous strain for experiments at (*a*) −10°C and (*b*) −20°C. Creep stress levels are indicated in the keys.

increasing brine content, in keeping with previous findings (Cole 1998). At the lower creep stress levels, ϕ and ρ generally changed little from their initial values as a result of straining up to $\varepsilon_{\text{creep}} \approx 0.01$.

With regard to the quantities plotted together in figure 3, it is emphasized that ρ and ϕ were calculated from the cyclic loading response, whereas $\dot{\varepsilon}_{\text{visc}}$ and $\varepsilon_{\text{anelastic}}$ were determined from the creep response. Employing these two experimental methodologies thus provides independent measures of the state of the specimen. The fact that the quantities plotted in the figure all exhibit similar strain dependences strongly suggests that they are influenced by a common underlying mechanism.

Lower creep stresses were applied to the specimens tested at higher temperatures to avoid catastrophic failure. Interestingly, only the two specimens NP22 and NP23 that experienced higher stresses at −5°C showed an increase in the dislocation density with increasing straining; the dislocation density for specimens tested under lower creep stress levels actually decreased during straining. Presumably the latter specimens NP14 and NP32 were experiencing dynamic recovery. Since Hiki and Tamura (1981) found that the dislocation density can vary simply as a function of time at high temperatures, some temporal variability in the dislocation density might be expected in the −5°C results.

The creep loading sequence was varied for specimen A74.B3 in a way that was designed to test the dislocation glide theory of viscous straining. For this specimen,

the creep segments consisted of an initial series of increasing compressive stress levels (−0.1, −0.2, −0.3, −0.4, −0.5 and −0.8 MPa), immediately followed by a second series of −0.1, −0.3, −0.5, and −0.8 MPa creep loading segments. The intent of applying the second set of creep stresses was to determine whether the stated loading history would alter the power law behaviour that is observed on previously unstrained specimens. Given that a high dislocation density was established during the first set of creep loadings (up to 0.8 MPa), the dislocation density should remain relatively high during the application of the lower stress levels in the second set of

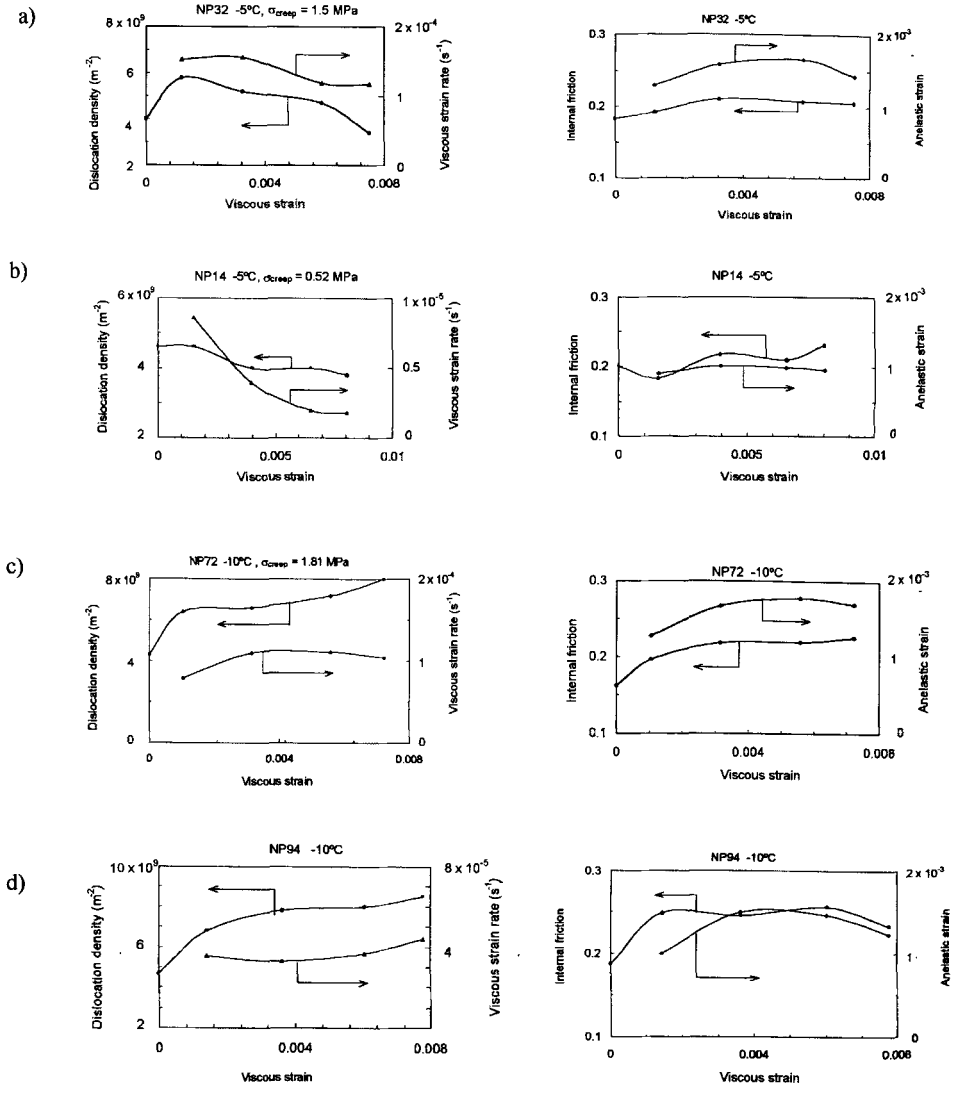

Figure 3. Representative plots of dislocation density and viscous strain rate versus viscous strain (shown on the left), and internal friction and anelastic strain versus viscous strain (shown on the right), for various temperatures: (*a*), (*b*) −5°C; (*c*), (*d*) −10°C; (*e*), (*f*) −15°C; (*g*), (*h*) −20°C. The test temperature and applied creep stress level follow the specimen name.

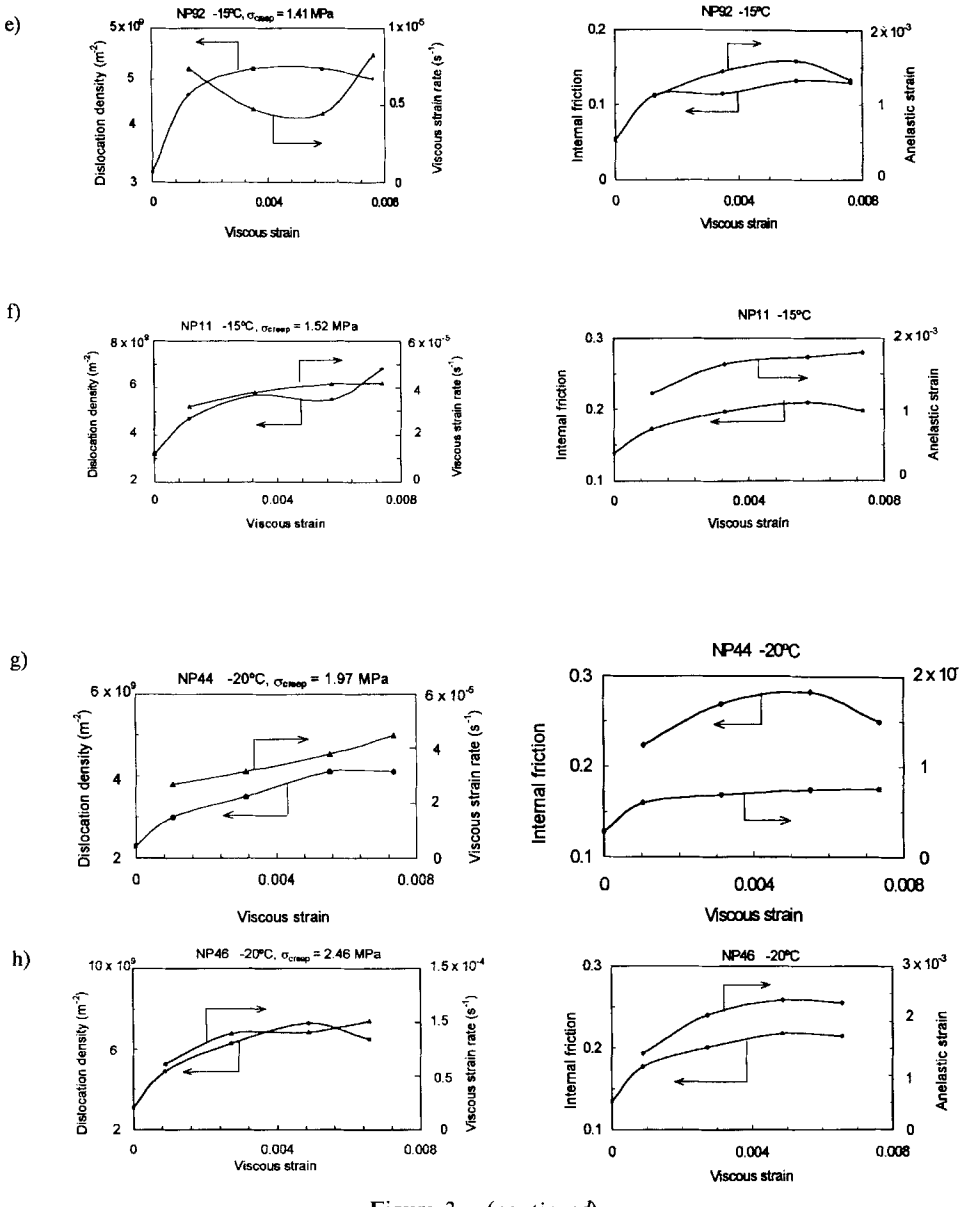

Figure 3. (*continued*)

loadings. Apart from dynamic recovery effects, the dislocation density is thus expected to be relatively independent of the applied stress during the second series of creep loadings. This circumstance provides an important test of the applicability of the glide-based theory of ice deformation, as discussed in greater detail in a subsequent section.

The specimen was a field core of aligned first-year sea ice from the Alaskan Arctic. The loading direction coincided with the preferred *c*-axis direction, producing a relatively low resolved shear stress on the basal planes. As a consequence, this

specimen exhibited a substantially lower creep rate than the unaligned laboratory-prepared specimens that are otherwise being presented. The test temperature for this specimen was −5°C.

Cyclic loads applied before, between and after each creep segment provided a way to calculate the anelastic compliance of the specimen and thereby to track changes in the effective dislocation density. Significantly, the cyclic loading response provided a means to monitor reductions in the number of dislocations (due to dynamic recovery) under low stresses and during breaks in the testing, as well as increases in their number under higher stresses.

Figure 4 shows plots of the viscous strain rate versus creep stress and the calculated dislocation density versus accumulated viscous strain. The salient point is that the prior deformation altered the power law behaviour. The slope of the viscous strain rate versus creep stress relationship (in log–log space) was about 3 during the initial set of increasing creep stresses and dropped to about 1 when reloaded (figure 4(*a*)). An analysis of the cyclic loading response indicated that the calculated dislocation density increased during the initial set of increasing creep stresses and remained nearly constant during the second set (figure 4 (*b*)). The dislocation density shows evidence of recovery when the time between loadings was a day or more. The implications of these initial findings are discussed in a subsequent section. Follow-up experiments that verify these initial findings for other ice types have been performed and will be presented in a subsequent paper.

The above testing sequence was lengthy, and the experiment was interrupted several times (one 3 day period and two 1 day periods), as indicated in figure 4 (*b*). The interruptions provided an opportunity to gain insight regarding post-straining recovery processes. An analysis of benchmark sets of load cycles applied before and after each interruption indicated that the dislocation density dropped by about 25% during the 3 day period, and by 3.7 and 7% in the 1 day periods, indicating that recovery processes were operating.

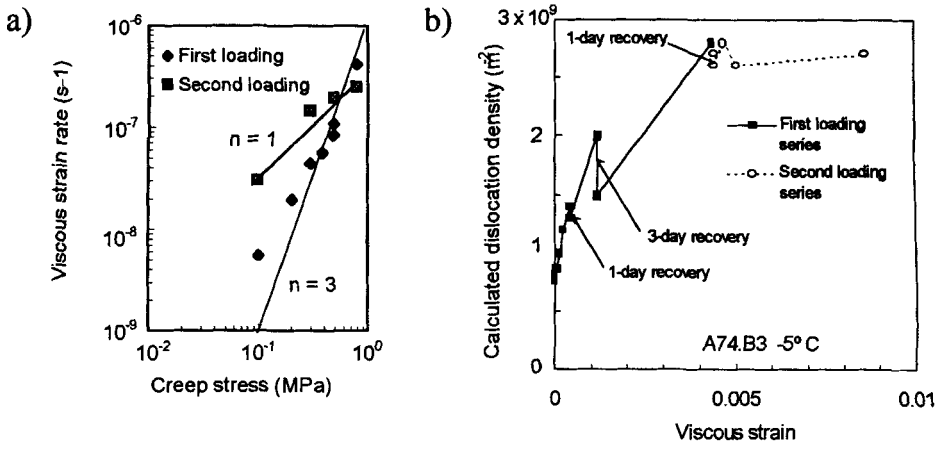

Figure 4. Results from staged creep experiments on a field core of aligned first-year sea ice (specimen A74.B3). (*a*) Strain rate versus creep stress for both loading sequences. Lines with slopes of 1 and 3 are inserted for reference. (*b*) Calculated dislocation density versus accumulated viscous strain for the two creep loading series described in the text. The 1 day and 3 day recovery periods are noted.

§ 5. Analysis

5.1. *Dislocation density determination*

The cyclic loading response provides a snapshot of a specimen at a particular point in its loading history, and the dislocation-based model described by Cole (1995) and Cole *et al.* (1998) provides a means to calculate an effective mobile dislocation density from that response. At the loading frequency of 10^{-1} Hz, grain-boundary relaxation is virtually in phase with the applied load and makes an insignificant contribution to the observed hysteresis loop area. In addition, the loading times are too short and the applied stress levels are too low for significant viscous straining to occur. Under these loading conditions, the hysteresis loop area is proportional to the mobile dislocation density. The effective dislocation densities were estimated from the hysteresis loop areas using the model of Cole (1995), which gives the loss compliance due to dislocations as D_2^{d}:

$$D_2^{\mathrm{d}} = \alpha^{\mathrm{d}}\,\delta D^{\mathrm{d}}\,\frac{1}{\exp(\alpha^{\mathrm{d}} s) + \exp(-\alpha^{\mathrm{d}} s)}, \tag{1}$$

where

$$\delta D^{\mathrm{d}} = \frac{\rho \Omega b^2}{K}. \tag{2}$$

In these expressions, $s = \ln(\tau\omega)$ (τ is the temperature-dependent relaxation time for the dislocation mechanism and ω is the angular frequency of loading). Equation (1) describes a relaxation process and the mathematics are such that the term α^{d} governs the width of the relaxation peak while keeping its area constant. α^{d} is determined from experimental data in the frequency domain and its value is controlled by the distribution of dislocation relaxation times. Ω is an orientation factor that converts the background normal stress to the average resolved shear stress on the basal planes ($\Omega = 0.32$ for polycrystalline ice with randomly oriented grains), $\alpha^{\mathrm{d}} = 0.56$ for saline ice, ρ is the dislocation density in reciprocal square metres, b is the magnitude of the Burgers vector (4.52×10^{-10} m) and K is the restoring stress constant (0.07 Pa). Thus, the quantities α^{d}, K, τ, ω and Ω are either known or can be estimated reasonably well.

A computer program based on the anelastic straining model of Cole (1995) has been developed. One of its capabilities is the calculation of hysteresis loops for sinusoidal loading, based on the frequency and amplitude of the stress cycles, temperature, microstructural characteristics and gas porosity. In the case of aligned ice, the degree of alignment and the orientation of the axis of loading to the preferred c-axis direction can be specified. In the case of sea ice, either the bulk salinity or the brine porosity can be specified as well. The program provides estimates of the initial mobile dislocation density given the ice type and, in the case of sea ice, the salinity, or initial values can be specified. Since the present analysis essentially required a back calculation of the dislocation density from the hysteresis loop area, the model was used to generate a relationship between the hysteresis loop area and the dislocation density with other input as prescribed by the ice type and experimental conditions. This relationship was then used to determine the effective dislocation density from the observed loop areas. Care was taken to assure that the model predictions of the effective elastic behaviour were in line with observations as well.

The plots on the left-hand side of Figure 3 show the viscous strain dependence of the mobile dislocation density as determined from the responses of the specimens to each set of loading cycles, together with the viscous strain rate. The plots on the right-side of figure 3 show the corresponding values of internal friction and anelastic strain as a function of viscous strain.

The following sections examine the experimental results to shed light on the changes in dislocation density as a function of the creep stress level, accumulated viscous strain and temperature. Although the experiments focus on saline ice, granular and columnar freshwater ice results are included to highlight the influence of microstructure on the dislocation density that develops under a given stress history.

5.2. *Threshold stress for dislocation multiplication*

The staged creep testing method offers an important advantage for studying the transition from $n = 3$ power-law to linear viscous behaviour. In traditional creep experiments, a specimen is strained continuously and the strain rate of interest is determined from the derivative of the total strain–time curve. There is a perennial concern that the minimum strain rates (typically in the range 10^{-7}–$10^{-9}\,s^{-1}$) measured at low stresses could be inappropriately high owing to transient strain effects. The staged creep-testing method avoids this problem since it isolates the transient and viscous components of strain for each segment of the experiment.

The creep stress levels were sufficiently high to cause the dislocation density to increase significantly (approximately by a factor of two) from its initial level for virtually all but the lower stress experiments at −5°C. The observation that the effect of straining on the calculated dislocation density diminishes as the creep stress level decreases (see figures 2 (*a*) and (*b*)) suggests that a threshold is being approached and that the dislocation density may be independent of strain below a certain stress level. Evidence from traditional creep experiments suggests that the onset of $n = 3$ power-law behaviour occurs in previously unstrained saline ice near a creep stress of approximately 0.25 MPa (Richter-Menge and Cox 1995). Although the creep stress range in most of the present experiments did not extend to sufficiently low stresses to capture this transition, as discussed above, there is some indication that the transition is being approached as σ_{creep} decreased to 0.3 MPa. The results from specimen A74.B3 (subjected to two series of increasing creep stresses) provide a strong, albeit preliminary, indication that the threshold stress for the shift from $n = 1$ to $n = 3$ behaviour increases as a result of prior straining. This observation indicates that the threshold stress for $n = 3$ behaviour depends on the prevailing dislocation density. The lower transition stress for freshwater ice (data summarized in the paper by Langdon (1973) indicate a value of approximately 0.1 MPa) is explained by the lower initial dislocation density that is typical of that material.

5.3. *Microstructure and pre-strain effects*

It is useful to examine results from freshwater granular and columnar ice to put the saline ice observations into perspective. The freshwater ice results will be covered in detail at a later date. Figures 5 (*a*) and (*b*) plot the calculated dislocation density and viscous strain rate as functions of viscous strain for a columnar and a granular freshwater ice specimen respectively under the conditions indicated. The columnar specimen was cut so that its loading axis made an angle of 45° with the growth direction to maximize the resolved shear stress along the growth direction (and thus the long dimension of the columnar grains). Although the magnitudes were some-

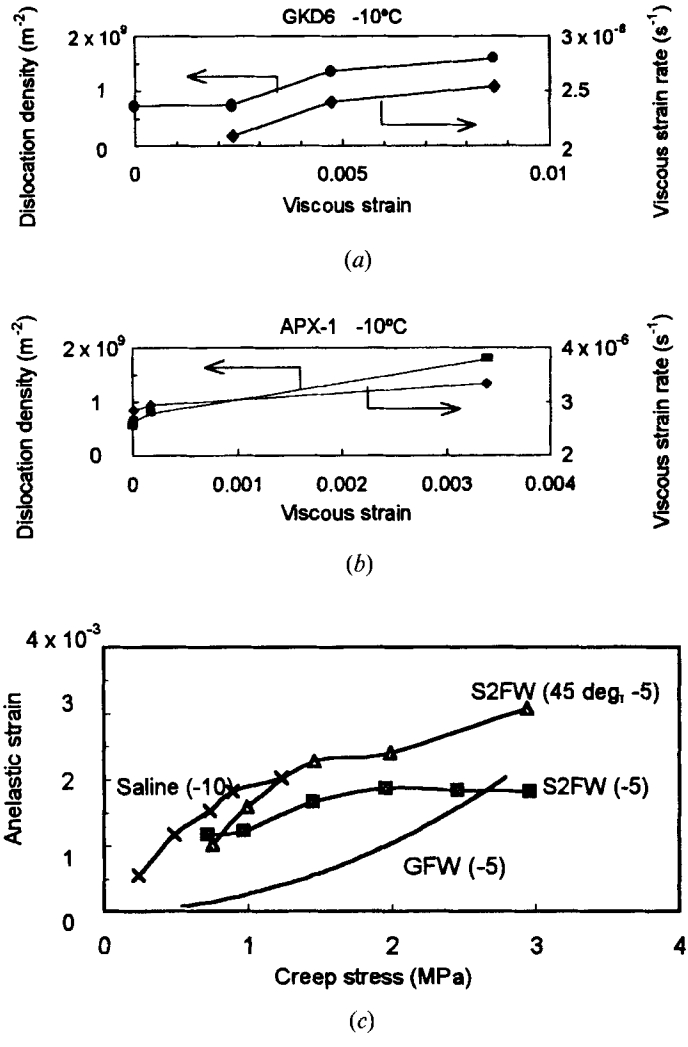

Figure 5. (*a*), (*b*) Dislocation density and viscous strain rate versus accumulated viscous strain for (*a*) a columnar-grained freshwater ice specimen (see text for details) and (*b*) a granular freshwater ice specimen. (*c*) Representative results of anelastic strain versus creep stress for the following: curve GFW (−5), granular freshwater ice at a test temperature of −5°C; curve saline (−10), saline ice at a test temperature of −10°C; curve S2FW (−5), laboratory-prepared S2 freshwater ice at a test temperature of −5°C; curve S2FW (45 deg, −5), laboratory-prepared S2 freshwater ice specimen that was cut with its loading axis oriented at 45° to the growth direction, and tested at a temperature of −5°C.

what lower, the calculated dislocation densities and viscous strain rates of the freshwater columnar specimens exhibited fundamentally the same strain dependence found in the saline ice specimens. Figure 5 (*c*) shows representative values of anelastic strain versus creep stress level for several ice types. The grain size of the columnar specimens was in the range 5–8 mm, whereas the granular ice curve is representative of material with grain sizes in the approximate range 1–5 mm. Anelastic strain is used in this comparison because the cyclic loading response necessary for an independent

estimate of the dislocation density was not obtained for some of these specimens. The GFW (−5) curve shows the trend for 38 data points for granular freshwater ice specimens (Cole 1991). The other curves are for individual specimens that were subjected to staged creep tests with a series of increasing stress levels.

The overall trend for creep straining to cause an increase in the dislocation density is apparent in each ice type. However, the results indicate that, firstly, under a given creep stress, saline ice exhibits a higher anelastic strain (and therefore dislocation density) than freshwater ice, secondly, a limiting value of ρ (and thus ϕ and $\varepsilon_{\text{anelastic}}$) is reached as stress increases, presumably as a result of microcracking, and, thirdly, in the case of saline ice, the applied creep stress appears to be best correlated with the increase in dislocation density, rather than with its absolute level. These results indicate that the dislocation density that ultimately develops depends on the initial microstructural characteristics of the specimen and is not simply a function of the creep stress. Consequently, saline and freshwater ice specimens subjected to a given creep stress level will develop different dislocation densities by the end of primary creep.

Although no systematic grain size dependence of the anelastic strain has emerged, grain size is expected to have at least an indirect effect through its influence over microcracking. As indicated in figure 5(*c*), anelastic strain does not increase indefinitely with increasing creep stress but appears to reach a plateau in some cases. It is believed that damage due to microcracking limits the anelastic strain that the microstructure can support and gives rise to the concave downward shape of all but the granular freshwater curve shown in figure 5(*c*).

5.4. *Temperature dependence of the dislocation density*

The dislocation density ρ in equation (3) is the sum of the initial value ρ_0 and the increase $\Delta\rho$ experienced during straining. An analysis of $\ln(\Delta\rho/\sigma)$ versus $1/T$ (K) for the data in table 2 indicates that $\Delta\rho$ is a function of temperature, with an apparent activation energy Q_ρ for dislocation multiplication of 0.45 eV (figure 6). The −5°C experiments that did not exhibit an increasing dislocation density have been omitted from this analysis. It is generally accepted that the dislocation density that ultimately develops under straining is proportional to $(\sigma/E)^2$ for many crystalline solids (Weertman 1983), where E is the elastic modulus. The temperature depen-

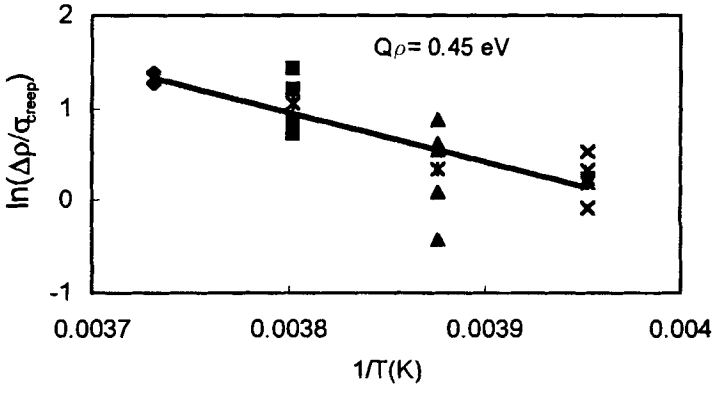

Figure 6. Natural logarithm of $\Delta\rho/\sigma_{\text{creep}}$ versus $1/T$ (K) for the data in table 2. Experiments at $T = -5$°C that did not show an increasing dislocation density have been omitted.

dence of this relationship for ice would not be significantly influenced by thermal effects on E (e.g. a ΔT of 10°C produces a 1.3% change in the average modulus of polycrystalline ice). However, since Orlová *et al.* (1972) found a mild temperature dependence of the dislocation density in aluminium (an apparent activation energy of 0.28 eV is estimated from their figure 5), there is some precedent for the temperature dependence observed for ice. The saline ice data for $T = -20$°C, which involved relatively high stress levels (up to about 3 MPa) and little specimen-to-specimen variation in physical properties, followed a $\Delta\rho \propto \sigma^2$ relationship. However, lower peak stresses were applied in the experiments at higher temperatures, and there were greater variations in the physical properties of these specimens. These factors make it difficult to ascertain the true stress dependence of $\Delta\rho$ at the higher temperatures and prompted use of $\ln(\Delta\rho/\sigma)$ in the activation energy analysis. Although the temperature dependence of $\Delta\rho$ is evident, it is cautioned that the above analysis is preliminary, and additional experiments and analysis are needed.

5.5. *Viscous straining*

The viscous strain rate was calculated for each segment of creep loading by dividing the non-recoverable strain observed for the segment by the time under load. Although constitutive models have generally taken the viscous strain rate as constant through primary creep (for example Sinha (1978) and Sunder and Wu (1989)), the results presented in figure 3 indicate that, for the prevailing conditions, the viscous strain rate typically increased as straining proceeded. Significantly, the changes in the viscous strain rate closely parallel the changes in the anelastic strain, the internal friction and the calculated dislocation density. Reflecting the trends in ρ, $\varepsilon_{\text{anelastic}}$ and ϕ, the viscous strain rate typically approached a nominally constant value toward the end of primary creep.

The shear strain rate associated with dislocation glide-controlled creep (for example Weertman (1983)) is given by

$$\dot{\gamma}_{\text{visc}} = \beta\rho b v, \tag{3}$$

where β is a numerical constant of order unity, ρ is the mobile dislocation density, b is the magnitude of the Burgers vector and v is the stress- and temperature-dependent dislocation velocity. Higashi *et al.* (1964) employed such a model in their analysis of the behaviour of ice single crystals. For drag-controlled glide, the dislocation velocity is

$$v = \frac{b\sigma_{\text{rss}}}{B(T)} \tag{4a}$$

where σ_{rss} is the resolved shear stress on the basal plane. The temperature-dependent drag term $B(T)$ is

$$B(T) = B_0 \exp\left(\frac{Q_{\text{glide}}}{kT}\right). \tag{4b}$$

Using an average dislocation mobility of $5.1 \times 10^{-12}\,\text{m}^3\,\text{N}^{-1}\,\text{s}^{-1}$ at -18°C, Cole (1995) determined a value of $B_0 = 1.205 \times 10^{-9}$ Pa s. The velocity term is thus

$$v = \frac{b\sigma_{\text{rss}}}{B_0} \exp\left(\frac{-Q_{\text{glide}}}{kT}\right), \tag{4c}$$

where Q_{glide} is the activation energy for basal glide (0.55 eV). Using the orientation factor Ω to convert the background normal stress σ_{creep} into the resolved shear stress, and substituting into equation (3) produces the following expression for the viscous shear strain rate:

$$\dot{\gamma}_{\text{visc}} = \frac{\beta\rho\Omega b^2\sigma_{\text{creep}}}{B_0}\exp\left(-\frac{Q_{\text{glide}}}{kT}\right). \tag{5a}$$

It is useful to express equation (5*a*) in terms of the equivalent strain rate in the direction of uniaxial loading for comparison with the experimental data. This conversion depends on the angle between the average slip plane and the loading direction. Cole *et al.* (1998) gave an expression for the orientation factor for a polycrystal of m grains, each with area a_i. If the total grain area is a, the applied stress makes an angle φ_i with the basal plane normal and an angle λ_i with the slip direction, the orientation factor is

$$\Omega = \sum_{i=1}^{m}\frac{a_i}{a}\cos(\lambda_i)\cos(\varphi_i),$$

where $a = \sum_{i=1}^{m} a_i$. Since the shear strain rate–axial strain rate conversion factor should scale with the orientation factor Ω, it is convenient to use $\Omega^{1/2}$. In the case when $\Omega = 0.5$, for example, which indicates that the plane of shear is optimally oriented (45°) to the axis of applied stress, the term $\Omega^{1/2}$ gives a factor of 0.707:

$$\dot{\varepsilon}_{\text{visc}} = \frac{\beta\rho\Omega^{3/2}b^2\sigma_{\text{creep}}}{B_0}\exp\left(-\frac{Q_{\text{glide}}}{kT}\right). \tag{5b}$$

Figure 7 shows a plot of the viscous strain rates predicted by equation (5*b*) versus the experimentally observed viscous strain rates for the data given in table

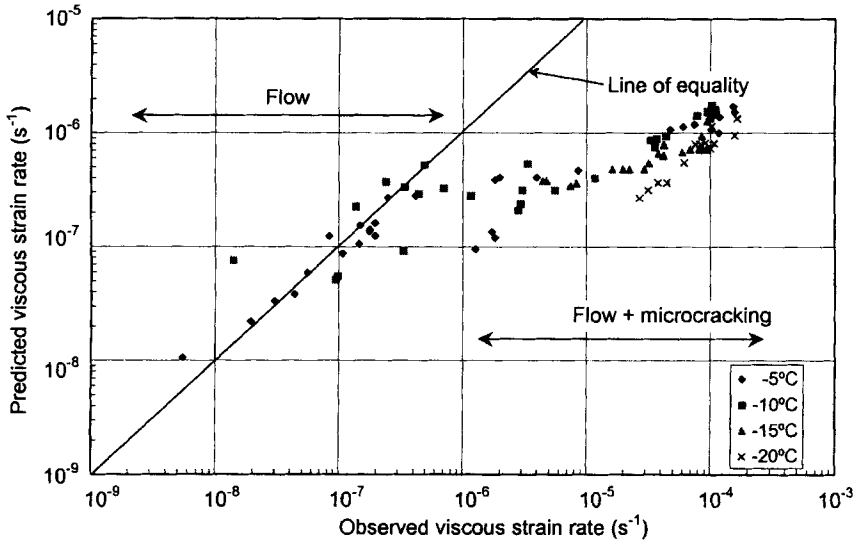

Figure 7. Strain rates predicted by equation (5*b*) versus observed strain rates for the data in table 2.

2. A best-fit analysis of the data for strain rates below $10^{-6}\,s^{-1}$ in figure 7 leads to a value of 0.3 for β in equation (5*b*). This value is in line with the expectation that β should be of order unity. Interestingly, the model predicts the viscous strain rates of both freshwater and saline ice specimens very well for strain rates up to about $10^{-6}\,s^{-1}$ but under-predicts the experimental results at higher viscous strain rates. Since this limit of applicability corresponds approximately to the onset of internal microcracking in most ice types, it is speculated that the model under-predicts the viscous strain rate because it does not account for the effects of microcracking. Unfortunately, microcracking activity was not monitored in these experiments, so it is difficult to address this matter quantitatively at this time.

5.6. *Activation energy considerations*

The preceding section indicated that a model of the viscous straining of ice can be based on the product ρbv in equation (3), where the dislocation velocity v is a function of temperature and linearly dependent on stress (see the review by Whitworth (1978), Fukuda *et al.* (1987) and Shearwood and Whitworth (1991)). Although the model cannot be unambiguously verified through its temperature dependence alone, it is nonetheless important to examine its consistency with the apparent activation energies observed in the experimental results presented here and the literature.

Reported values for the activation energy of the fundamental process of basal dislocation glide typically vary from 0.55 to 0.62 eV, depending on the experimental technique. On the other hand, the most commonly reported values for the activation energy for polycrystalline freshwater and saline ice in power law creep are in the range 0.7–0.81 eV (67–78 kJ mol^{-1}) (Homer and Glen 1978, Weertman 1983). The activation energy for anelastic straining during cyclic loading (where no new dislocations are produced) is in line with that of basal glide. However, the activation energy for the anelastic straining observed in creep recovery experiments (where new dislocations are produced) is approximately equal to that of viscous straining in the power-law regime. Significantly, the analysis presented above sheds light on these differences.

An analysis of the stress and temperature dependence of the viscous strain rates observed for the final creep loading segment of each specimen indicated that $n \approx 3$ power-law behaviour was obeyed. An analysis of data at all temperatures for which an increase in dislocation density was observed led to an apparent activation energy for viscous straining of 0.91 eV, and a value of 0.78 eV was obtained when the -5°C data were excluded. A similar analysis of the anelastic strain produced values of 0.87 eV for all temperatures, and 0.76 eV when the -5°C data were excluded.

Since $\Delta\rho$ in equation (5) is a function of temperature, the model predicts that the apparent activation energy for creep can, in the extreme, vary from Q_{glide} (0.55 eV) when $\Delta\rho = 0$, to $Q_{\text{glide}} + Q_\rho$ (1.0 eV) when $\Delta\rho \gg \rho_0$. The average values of ρ_0 and $\Delta\rho$ calculated from the data in table 2 lead to a value of $Q_{\text{apparent}} = 0.75$ eV, which is in good agreement with the observed value of 0.78 eV noted above.

The dislocation-based analysis predicts two other trends: firstly, a somewhat higher creep activation energy should be observed in the $n = 3$ regime than in the $n = 1$ regime; secondly, Q_{apparent} should increase with increasing stress in the $n = 3$ regime as $\Delta\rho$ increases relative to ρ_0. Interestingly, the freshwater ice literature contains support for these points. Figure 8(*a*) plots values of Q_{apparent} versus the stress exponent n obtained for polycrystalline freshwater ice (Homer and Glen 1978).

Since the temperature dependence evident in the flow regime is lost when power-law breakdown occurs, only data for $n \leqslant 3.3$ have been considered. The data in figure 8 (*a*) show a systematic increase in Q_{apparent} as n increases, as expected from the foregoing discussion. Figure 8 (*b*) shows a mild stress dependence of Q_{apparent} that was calculated from the raw data obtained by Ramseier (1972) for granular freshwater ice. It is difficult to develop a similar analysis for saline ice owing to the lack of a comprehensive data set and the added complication of its highly variable and temperature-dependent microstructure.

Significantly, the temperature dependence of $\Delta\rho$ explains the difference in activation energy for anelastic strain under cyclic loading (when no change in dislocation density occurs, $\Delta\rho = 0$) and creep (when the dislocation density increases, $\Delta\rho > 0$). Ignoring the minor contribution of grain-boundary sliding for the moment, the amount of anelastic strain observed under cyclic loading is governed by δD^{d} (equation (2)), which depends on the dislocation density ρ. This process exhibits an activation energy $Q_{\text{glide}} = 0.55\,\text{eV}$. The anelastic strain observed during creep recovery, on the other hand, has a predicted activation energy of 0.76 eV because of the contribution of the temperature dependence of the dislocation multiplication process. This

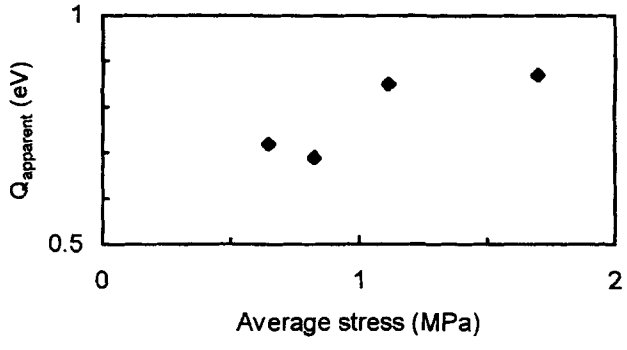

(*a*)

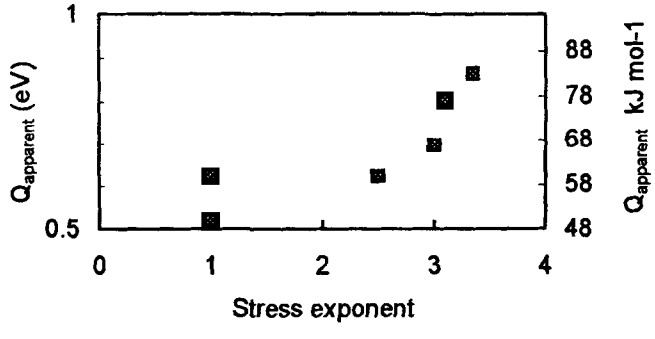

(*b*)

Figure 8. (*a*) Q_{apparent} versus the power-law stress exponent n for polycrystalline freshwater ice using data from various researchers, as summarized by Homer and Glen (1978). (*b*) Q_{apparent} versus creep stress for polycrystalline freshwater ice in the $n = 3$ power-law regime, calculated from the results of Ramseier (1972) for granular (snow) ice.

value is approximately equal to the experimentally observed value of 0.78 eV for viscous straining. Moreover, the predictions agree with longstanding observations in the literature regarding the apparent equivalence of the activation energies for viscous and anelastic straining during creep (Sinha 1978).

§ 6. Discussion

As noted above, the effort was motivated by a desire to understand better the dislocation basis for the deformation of ice, and thereby to improve the ability to generate a physically based constitutive model for this important material. The approach adopted here employed, firstly, the experimental capability to apply zero-mean-stress cycles in conjunction with quasistatic loading and, secondly, the analytical capability to arrive at an effective dislocation density based on the cyclic loading response. This approach produced quantitative information regarding the evolving dislocation density, as well as a consistent picture of the dislocation basis for viscous and anelastic straining. Ice is particularly amenable to this treatment because basal slip dominates the flow of ice in the regime of interest. The rate of flow is governed by the product of the density ρ of participating dislocations and their average velocity v. It is important to recognize that the analytical effort cannot uncouple these two quantities. Thus, to calculate an effective dislocation density, the analysis relies on the anelastic straining model of Cole (1995) which employs an average mobility taken from the literature. The adopted value is believed to be representative of basal dislocations of mixed character, but the mobilities reported in the literature are obtained from material having lower dislocation densities than are found in typical ice experiments. At this time, it is not known whether or the extent to which the average mobility might be influenced by the high dislocation densities that were achieved in the experiments reported here. The discovery that some other value of dislocation mobility applies would not alter the model in any fundamental way, but it would require compensating changes in the calculated dislocation density and mobility. The fact that the dislocation densities calculated by the model for freshwater ice specimens fall in the range of expected values† indicates that the model employs a realistic mobility value.

The ability to quantify dislocation processes during straining, and as a function of temperature and strain history, provides information regarding of the long-running uncertainty of the process that controls the stress versus minimum creep rate relationship of ice (see reviews by Weertman (1973, 1983), for example). The experimental finding that the viscous strain rate during primary creep shows a strong tendency to increase (or decrease) with dislocation density is commensurate with dislocation drag being the rate-controlling mechanism under the stated experimental conditions. The observation that the power law exponent depends on prior strain history, and the observed recovery effects, provide support for this view as well. Finally, an examination of the temperature dependence of viscous and anelastic straining was seen to reflect subtle but well documented changes in activation energy that are predicted on the basis of the glide theory with a temperature-dependent dislocation generation term. While it is difficult to identify a deformation mechanism unequivocally, the combination of strain history, stress level and temperature effects,

† After pre-straining single crystals in the range 0.15–0.30 MPa, Joncich (1976) estimated that ρ was of the 10^9 m^{-2} order of magnitude. Fukuda and Shoji (1981) also calculated values of ρ of the same order of magnitude.

together with the indications that the same fundamental dislocation processes operate in microstructurally different ice types, makes a strong case for a glide-controlled mechanism of viscous straining.

The agreement of the viscous straining equation (5*b*) with the experimental observations at low strain rates is very encouraging, as it relates characteristics of dislocation processes, temperature and microstructural characteristics to flow behaviour. By incorporating the dislocation density, it has the capacity to account explicitly for strain history effects. Although dislocation-based models have been employed primarily in the realm of ice physics, the present effort is intended to incorporate dislocation kinetics into a constitutive model that is applicable to larger-scale behaviour. Ongoing work is addressing the verification of the model with *in-situ* specimens on the scale of tens of metres.

The observation that the activation energy for polycrystalline ice creep is approximately equal to that for self-diffusion (0.62 eV) suggests to some that the minimum creep rate is diffusion controlled (for example Ramseier (1972)). However, as seen above, values reported for polycrystalline ice creep are typically higher than the diffusion value. On the diffusion-based interpretation, the rate at which ice deforms is limited by the rate at which the strain resulting from dislocation motion can be accommodated by diffusive processes. In the glide-controlled theory, on the other hand, deformation is controlled by the rate at which basal dislocations move. On this argument, even though the dislocation strains are ultimately accommodated by diffusion, it is the product of the number of dislocations and their average rate of travel that determine the overall creep rate. Glide-controlled creep has long been recognized as a viable mechanism for ice (Weertman 1963) because of the exceptionally high intrinsic drag on basal dislocations. Interestingly, creep rate calculations based on a glide-controlled process are in excellent agreement with observations, but unequivocal evidence in support of that mechanism has not previously been produced.

The glide-controlled theory indicates that if the applied stress is sufficiently low, dislocations do not multiply (e.g. $\Delta\rho = 0$), and linear ($n = 1$) behaviour and the activation energy of basal glide (0.55 eV) should be observed. A transition to $n = 3$ behaviour begins when the stress becomes high enough to cause dislocation multiplication ($\Delta\rho > 0$), at which point the temperature dependence of the dislocation multiplication process becomes manifest. The apparent activation energy consequently increases as the relative contribution of the newly generated dislocations to the total population increases. It is interesting that the temperature dependence of the dislocation multiplication process noted above (Orlová *et al.*, 1972) was ignored because its magnitude was small compared with the overall activation energy for creep in aluminium. For the case of ice, however, this contribution is significant and appears to explain several apparent inconsistencies in the temperature dependence of both the anelastic and the viscous components of strain.

Although the above analysis indicates that diffusion is not the rate-controlling mechanism in primary creep, the rate of recrystallization, which is diffusion controlled, is expected to play an important role after the minimum creep rate occurs (at an axial strain of about 0.01).

§ 7. Summary and conclusions

An analysis of cyclic and creep loading experiments on sea ice specimens indicates that $n \approx 3$ power-law behaviour is observed when the applied stress controls

the effective dislocation density, and that $n \approx 1$ when the dislocation density is effectively independent of stress. A preliminary experiment demonstrated that prior straining resulted in approximately linear behaviour at stresses that are usually associated with $n = 3$ behaviour. A temperature dependence of the dislocation generation mechanism emerged, which gives a physically based explanation for the difference between the activation energy for polycrystalline ice creep and that of basal glide. The dislocation-based anelastic straining model of Cole (1995, 1998) provided a means to calculate the effective dislocation densities from the cyclic loading response of the specimens. The findings offer a range of support for a dislocation glide-controlled mechanism for viscous straining in saline ice.

By combining cyclic and creep loading methods, the effective dislocation density can be determined as a function of creep deformation history. For temperatures in the range from -10 to -20°C and compressive creep stresses above 0.5 MPa, the calculated mobile dislocation density, anelastic strain and viscous strain rate typically increase during primary creep. Despite some scatter, the experiments show that the viscous strain rate is a linear function of the mobile dislocation density. When a threshold stress was exceeded, the dislocation density was found to be a function of the applied creep stress, viscous strain level and temperature. The dislocation density increased to a plateau or apparently steady-state value during primary creep. The steady-state dislocation density was temperature dependent, with an apparent activation energy of 0.45 eV, and this was shown to explain the difference between the activation energy for basal glide (in the absence of dislocation multiplication) and the apparent activation energy for polycrystalline ice creep in the power law regime.

Dynamic recovery occurred during creep straining at $T = -5$°C for $\sigma_{creep} = 0.3$ MPa, as evidenced by a decrease in the calculated dislocation density during straining. Additionally, measurable post-straining recovery (a decrease in the dislocation density) occurred over periods of 1–3 days at -5°C. This finding illustrates that the time after straining is an important consideration in the application of the methodologies described above.

The above observations, coupled with the finding that the viscous strain rate is typically proportional to the prevailing dislocation density, support a dislocation glide-controlled mechanism of ice creep in the regime of flow with no internal cracking. A viscous straining model based on that mechanism was shown to reflect adequately the experimental findings.

Acknowledgements

The experimental work was conducted under the Office of Naval Research's Sea Ice Mechanics Initiative, and the support of Dr Thomas Swean, Dr Thomas Curtin and Dr Yapa Rajapakse is greatly appreciated. The US Army Cold Regions Research and Engineering Laboratory provided additional support. We acknowledge helpful discussions with Professor Ian Baker of Dartmouth College, Hanover, New Hampshire, and the assistance of Nancy Perron for her help in preparing the specimens and in conducting the physical properties characterizations.

References

Barrett, R., Baruchel, J., Hartwig, J., and Zontone F., 1995, *J. Phys.* D, **28**, A250–A255.

Cole, D. M., 1991, *Proceedings of the sixth International Specialty Conference on Cold Regions Engineering*, West Lebanon, New Hampshire, USA, 1991, edited by D. Sodhi, pp. 504–

518; 1993, *Proceedings of the Joint ASCE–ASME–SES Conference, Ice Mechanics 1993*, AMD-Vol. 163 (New York: American Society of Mechanical Engineers), pp. 261–272; 1995, *Phil. Mag.* A, **72**, 231; 1998, *Int. J. Solids Struct.*, **35**, 4067.

COLE, D. M., and DURELL, G. D., 1995, *Phil. Mag.* A, **72**, 209; 1998, *Proceedings of the IAHR 14th Symposium on Ice*, Potsdam, New Hampshire, USA, 1998, (International Association of Hydraulic Research) Vol. 2.

COLE, D. M., and GOULD, L. D., 1990, *Cold Regions Sci. Technol.*, **18**, 295.

COLE, D. M., JOHNSON, R. A., and DURELL, G. D., 1998, *J. geophys. Res.*, **103**, 21 751.

FUKUDA, A., and HIGASHI, A., 1969, *Proceedings of the International Symposium on the Physics of Ice*, edited by N. Riehl, B. Bullemer and H. Engelhardt (New York: Plenum) pp. 239–250.

FUKUDA, A., HONDOH, T., and HIGASHI, A., 1987, *J. Phys., Paris*, **48**, C1–163.

FUKUDA, A., and SHOJI, H., 1981, *Cold Regions Sci. Technol.*, **4**, 175.

HIGASHI, A., KOINUMA, S., and MAE, S., 1964, *Jap. J. appl. Phys.*, **3**, 610.

HIKI, Y., and TAMURA, J., 1981, *J. Phys., Paris*, Suppl 10, **42**, C5–547.

HOMER, D. R., and GLEN, J. W., 1978, *J. Glaciol.*, **21**, 429.

HU, X., BAKER, I., and DUDLEY, M., 1996, *Scripta mater.*, **34**, 491.

JONCICH, D. M., 1976, PhD Thesis, University of Illinois at Urbana-Champaign, Illinois, 97 pp.

LANGDON, T. G., 1973, *Physics and Chemistry of Ice*, edited by E. Whalley, S. J. Jones and L. W. Gold (Ottawa: Royal Society of Canada), pp. 356–361.

ORLOVÁ, A., TOBOLOBÁ, Z., and ČADEK, J., 1972, *Phil. Mag.*, **26**, 1263.

PICU, R. C., GUPTA, V., and FROST, H. J., 1994, *J. geophys. Res.*, **99**, 11 775.

RAMSEIER, R. O., 1972, PhD Thesis, Dartmouth College, Hanover, New Hampshire, 243 pp.

RICHTER-MENGE, J. A., and COX, G. F. N., 1995, *Proceedings of the Fifth International Offshore and Polar Engineering Conference*, The Hague, The Netherlands, Vol. II, pp. 312–316.

SHEARWOOD, C., and WHITWORTH, R. W., 1991, *Phil. Mag.* A, **64**, 289.

SINHA, N. K., 1978, *Exp Mech.*, **18** (12), 464.

SUNDER, S. S., and WU, M. S., 1989, *Cold Regions Science Technol.*, **16**, 45.

VASSOILLE, R., MAI, C., and PEREZ, J., 1978, *J. Glaciol.*, **21**, 375.

WEERTMAN, J., 1963, *Ice and Snow: Properties, Processes and Applications*, edited by W. D. Kingery (Cambridge, Massachusetts: MIT Press), pp. 28–34; 1973, *Physics and Chemistry of Ice*, edited by E. Whalley, S. J. Jones and L. W. Gold (Ottawa: Royal Society of Canada), pp. 320–337; 1983, *A. Rev. Earth planet. Sci.*, **11**, 215.

WHITWORTH, R. W., 1978, *J. Glaciol.*, **21**, 341.